Dynamical characterization of vibrating afm cantilevers forced by photothermal excitation

Dynamical characterization of vibrating AFM cantilevers forced by photothermal excitation

Valerio Pini,[1,*] Bruno Tiribilli,[2,3] Cecilia Maria Cristina Gambi,[4] and Massimo Vassalli[3,5]
[1]*BioNanoMechanics Laboratory, National Center for Microelectronics, IMM-CNM (CSIC), Calle Isaac Newton 8 (PTM), Tres Cantos, E-28760 Madrid, Spain*
[2]*Istituto dei Sistemi Complessi, Consiglio Nazionale delle Ricerche, Via Madonna del Piano 10, Sesto Fiorentino, I-50019 Firenze, Italy*
[3]*Centro Interdipartimentale per lo Studio delle Dinamiche Complesse, Via Sansone 1, Sesto Fiorentino, I-50019 Firenze, Italy*
[4]*Dipartimento di Fisica, Università degli Studi di Firenze, Via G. Sansone 1, Sesto Fiorentino, I-50019 Firenze, Italy*
[5]*Istituto di Biofisica, Consiglio Nazionale delle Ricerche, Via De Marini 6, Genova I-16149, Italy*
(Received 30 July 2009; revised manuscript received 2 December 2009; published 4 February 2010)

The detailed characterization of the dynamical behavior of an oscillating cantilever is a crucial task in many applications of scanning probe microscopy, force spectroscopy, and cantilever based biosensors. In the present work we considered a direct and localized excitation of the cantilever obtained using the photothermal effect induced by a modulated laser beam that allows us to completely separate the dynamics of the system from spurious effects. We developed a theoretical model able to describe the experimental results with high accuracy; in particular, a good agreement is achieved, both for amplitude and phase, in the presence of resonances and antiresonances, depending on the different location of the excitation beam.

DOI: 10.1103/PhysRevB.81.054302 PACS number(s): 78.20.N−, 46.40.−f, 07.10.Cm, 07.79.Lh

I. INTRODUCTION

Dynamic atomic force microscopy (AFM) has become a powerful tool for the nanoscale imaging and force spectroscopy of samples with very high resolution.[1] In dynamic AFM, the amplitude and phase of the oscillating tip represent the typical feedback control parameters that allow obtaining quantitative information on the topological and physical properties of the sample.[2] The key point in dynamical AFM techniques is the method used to produce the cantilever excitation. In the present work, the optical excitation method produced by an intensity modulation of a laser focused on the cantilever[3,4] has been studied. This excitation method has recently been implemented for high-speed microscopy applications of biomolecular processes,[5,6] and it demonstrated to be even more suitable for spectroscopy[7] and biosensing applications.[8] The optical method has the advantage to produce the excitation directly onto the cantilever, allowing a frequency response unaffected by spurious contributions of noise produced by the mechanical coupling with the other experimental components.[9] This feature offers the possibility to have a deep insight into the details of the system dynamics.[10,11]

Our attention has been focused on coated cantilevers, for which the main contribution to the excitation is due to the photothermal effect.[12] We treated the problem theoretically, finding an analytical solution for the spectral response of the cantilever that we compared with experimental results obtained on a customized AFM system.

II. MATERIAL AND METHODS

A. AFM setup

In Fig. 1(a) a picture of the custom built AFM apparatus used for the experiments is reported; in Fig. 1(b) an enlarged picture of the AFM head is shown. The cantilever deflection is measured with the optical beam deflection method (OBDM) where a laser diode (LD) beam is focused by an optical system on the back of the cantilever (near the free end) and the reflected beam is collected into a four quadrants detector [photodiode (PD)]. Two mirrors $M1$ and $M2$, fixed on the arms of a fork [see Fig. 1(b)] are used to deflect the laser beam toward the cantilever situated at a lower plane with respect to the other optical elements. This geometry (for more details see experimental setup in Ref. 13) permits to implement the OBDM without introducing mechanical elements above the cantilever, allowing a full optical access along the vertical axis. This feature permits to vertically focus a second laser beam [in the following referred to as excitation laser (EX) laser] on the cantilever for optical excitation [see Fig. 1(a)]. A commercial laser diode (mod.*LFX* from *Lasermax*, wavelength 670 nm) whose intensity can be modulated in analog mode from dc up to 3 MHz was used. In order to reduce the excitation beam size an optical microscope (mod.*FS*60 from *Mitutoyo*) was placed along the optical path; in this way it has been obtained a circular beam shape with a diameter of ≈ 5 μm. Scattered light from the EX laser, together with the environmental light, can generate noise on the four quadrants detector thus an optical narrowband filter (*Lot-Oriel*, wavelength 635 nm, spectral width 10 nm) was mounted at the input of the photodiode, matching the peak wavelength of the detection laser diode.

The mechanical head was mounted on a three axis closed-loop piezoflexure (mod.*PI*—527.3*CL* from *Physik Instrumente*) allowing the positioning of the focused beam along the cantilever with submicrometric accuracy.

The experiments reported in the following were performed using a commercial silicon gold coated cantilevers (mod. *CSG*01 from *NT-MDT*) with declared dimensions of: length 350 ± 5 μm; width 35 ± 3 μm; thickness 1.0 ± 0.3 μm. The errors declared on L and W were reasonably low to use these values in the theoretical model (in particular, the model is not much sensitive to W). Differently, the thickness T strongly affects the frequency position of the resonances and the error on it declared by the manufacturer is far enough to obtain a good comparison between experimental and theoretical data. The thickness T was determined

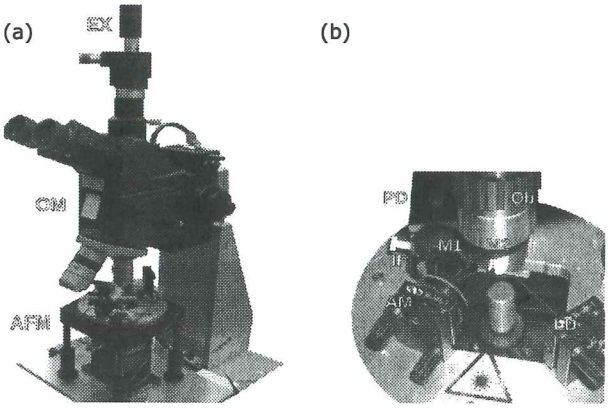

FIG. 1. (Color online) Custom-built AFM system. (a) A photograph of the entire AFM apparatus showing the mechanical head (AFM) and the optical microscope (OM) used to focus the EX on the cantilever back. (b) Enlarged view of the AFM head. The light emitted by the LD is deflected by a mirror ($M1$) toward the cantilever and reflected by its upper face toward a second mirror $M2$ (symmetric to $M1$); using an adjustable mirror (AM), the laser is than sent to the four quadrants photodiode (PD) for deflection and torsion measurements. An interference filter (IF) in front of the PD eliminates any contribution to the deflection signal coming from the environmental illumination and from the EX laser (focused by the objective Ob on the back of the cantilever).

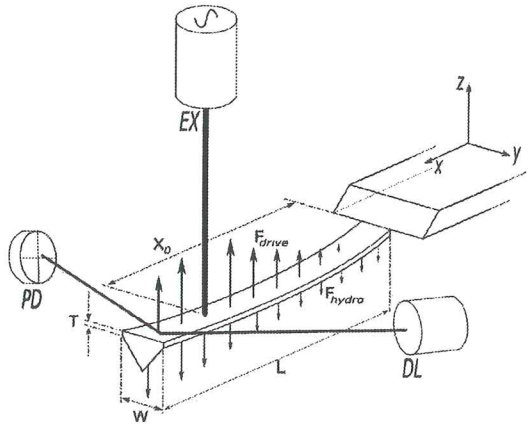

FIG. 2. Schematic drawing of a cantilever subject to a damping force F_{hydro} (down arrows) and external forces F_{drive} (up arrows). The main parameters used in the text are identified in the drawing: L=length, W=width, T=thickness, and x_0 is the distance of the excitation beam from the cantilever base. The relative positions of the EX laser, the PD, and the detection laser (DL) are reported.

starting from the knowledge of the first experimental resonance (for more details see Ref. 14).

B. Detection scheme

EX laser was sinusoidally modulated using a wave form generator (mod.33220*A* from *Agilent*) producing a periodic oscillation of the cantilever. The deflection four quadrants signal was compared with the EX laser driving signal by means of a lock-in amplifier (mod.9210 from *Princeton Applied Research*) that measures the amplitude A and the phase difference Θ between the two signals. Each measure was averaged in order to reduce statistical errors that can significantly affect the measurements, especially the phase measurements near the antiresonances of the spectrum.

In Fig. 2 a drawing of the system under study is presented where all the fundamental elements are sketched and the geometrical quantities and spatial coordinates are identified.

III. THEORETICAL MODEL

A. Cantilever dynamics

The dynamics of a cantilever forced to oscillate in a viscous fluid can be described by introducing two force fields (see Fig. 2): the hydrodynamic load F_{hydro} due to the dissipative motion of the beam in the fluid and F_{drive} representing the external driving force. To obtain the displacement of the cantilever $z(x,t)$ it is convenient to switch to a Fourier space description that, following the work presented in Ref. 15, leads to

$$EI\frac{\partial^4 Z(x|\nu)}{\partial x^4} - 4\pi^2\nu^2\rho A Z(x|\nu) = F_{hydro}(x|\nu) + F_{drive}(x|\nu), \tag{1}$$

where E is the Young's modulus, A is the cantilever cross section, I is the area moment of inertia,[16] ρ is the mass density, and ν is the frequency. The hydrodynamic load $F_{hydro}(x,\nu)$ can be written as[15]

$$F_{hydro}(x|\nu) = \pi^3\rho_f\nu^2W^2\Gamma(\nu)Z(x|\nu), \tag{2}$$

$\Gamma(\nu)$ being the hydrodynamic function for a rectangular beam, W is the cantilever width, and ρ_f is the mass density of the fluid.

The solution can be found by decomposing the deflection $Z(x|\nu)$ on the orthonormal basis of the normal modes $\phi_n(x)$ of the free cantilever[17,18]

$$Z(x|\nu) = \sum_{n=1}^{\infty} c_n(\nu)\phi_n(x), \tag{3}$$

where $c_n(\nu)$ are the frequency-dependent coefficients to be determined.

Using the orthonormalization property of normal modes $\phi_n(x)$,[19] inserting Eqs. (2) and (3) into Eq. (1) leads to the following equation for $c_n(\nu)$ coefficients:

$$c_n(\nu) = \frac{\int_0^L F_{drive}(x|\nu)\phi_n(x)dx}{EI\left\{\int_0^L\left[\frac{d^2\phi_n(x)}{dx^2}\right]^2 dx - B(\nu)\int_0^L[\phi_n(x)]^2dx\right\}}, \tag{4}$$

where $B(\nu)$ is given by

$$B(\nu) = \frac{4\pi^2 \rho A \nu^2}{EI}\left(1 + \frac{\pi W^2 \rho_f}{4A\rho}\Gamma(\nu)\right).$$

It is worth noting that the deflection detection method used in the system, the OBDM, does not give a direct measurement of the vertical displacement Z but it provides information on its spatial derivative, the deflection. For this reason, in the following paragraph, for the comparison with the experimental results, the following equation has been considered:

$$\frac{\partial Z(x|\nu)}{\partial x} = \sum_{n=1}^{\infty} c_n(\nu)\frac{d\phi_n(x)}{dx} \tag{5}$$

that should be evaluated at the laser detection position ($x=DL_{pos}$). This equation can be also written by making explicit its complex nature:

$$\left.\frac{\partial Z(x|\nu)}{\partial x}\right|_{x=DL_{pos}} = \sum_{n=1}^{\infty} a_n(\nu)e^{i\theta(\nu)} = A(\nu)e^{i\Theta(\nu)}, \tag{6}$$

where $A(\nu)$ is the cantilever amplitude oscillation (at the laser detection position) while $\Theta(\nu)$ represents the phase difference between the EX laser signal and the four quadrant signal deflection.

B. Photothermal effect

In order to solve Eq. (4) for a specific driving force it is necessary to write it into an analytical form. The presence of the EX laser induces several effects but, in the case of coated cantilevers, the leading phenomenon is the photothermal effect.[3,4] The intensity-modulated light, focused onto a region of the cantilever, produces a time-dependent temperature distribution due to the absorption of optical energy that induces a differential longitudinal stress across the cantilever thickness. This effect results in a significant bending for coated cantilevers due to the difference in the thermal expansion coefficients of the bulk and coating.

The derivation of the driving force generated by the photothermal effect has been described in Ref. 12. To evaluate the analytical form of the photothermal effect the following approximations have been assumed:

(i) The spatial and temporal coordinates are separable, so the driving force can be expressed by the following relation $F_{drive}(x|t)=f(x)g(t)$.

(ii) The temperature distribution is only dependent on the longitudinal coordinate x.

(iii) The temporal dependence of the driving force is sinusoidal, i.e.,

$$g(t) = \sin[2\pi\nu(t+t_0)],$$

where t_0 represents the temporal delay between the EX laser signal and the cantilever deflection.

As discussed in Ref. 12, these hypotheses are reasonable also for our experimental setup and the force induced by the photothermal effect can be written as

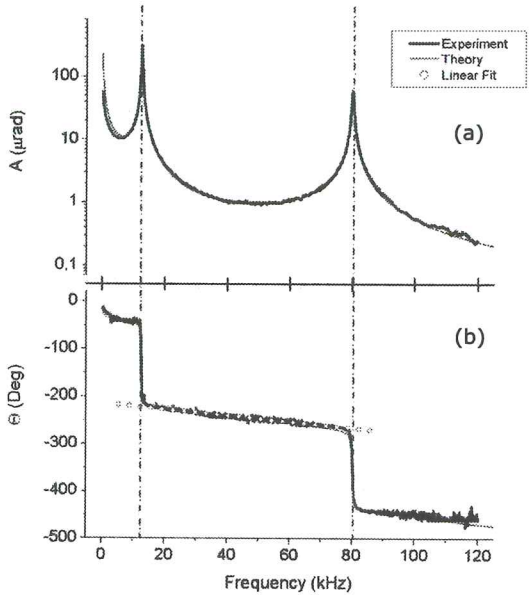

FIG. 3. (Color online) Experimental (thick line) and theoretical (thin line) frequency response of the amplitude A [panel (a)] and phase Θ [panel (b)] obtained with the EX laser near the base; theoretical calculations are obtained for $L=350$ μm, $T=1.3$ μm, and $x_0=0.1L$. The linear fit (empty circle) executed on a limited frequency region of the phase graph, gives a temporal delay equal to $t_0=(1.82\pm0.02)$ μs.

$$F_{drive}(x|\nu) = c_{th}(\nu)\frac{\partial^2}{\partial x^2}T(x,\nu)\delta(\nu-\nu_{ex})e^{i2\pi\nu t_0}, \tag{7}$$

where $T(x)$ is the spatial temperature profile produced on the cantilever, ν_{ex} is the excitation frequency, and c_{th} is a constant dependent on the geometrical and mechanical properties of the cantilever. The detailed calculation of $T(x)$ and c_{th} is reported in Ref. 12.

The temporal delay t_0 is related to many factors that cannot be *a priori* evaluated, thus it has been deduced from the experimental results.

IV. RESULTS

Figures 3–5 show the amplitude A [panel (a)] and phase Θ (panel B) curves obtained from the Eq. (6), together with the experimental data measured by the lock-in amplifier for three different positions of the EX laser on the cantilever: $x_0=0.1L$ (near the base, Fig. 3), $x_0=0.52L$ (in the middle, Fig. 4), and $x_0=0.76L$ (near the free end, Fig. 5).

The amplitude graphs show that the photothermal effect is highly efficient at low frequencies and also two resonance peaks are clearly visible for $\nu_0 \approx 12.6$ kHz and $\nu_1 \approx 79.8$ kHz. Making a comparison among the different amplitude graphs, it is clear that the photothermal excitation efficiency depends on the EX laser position x_0 and each cantilever mode has a different behavior with x_0; in Table I a complete list of the amplitude and frequency cantilever resonances and antiresonances for different x_0 are reported.

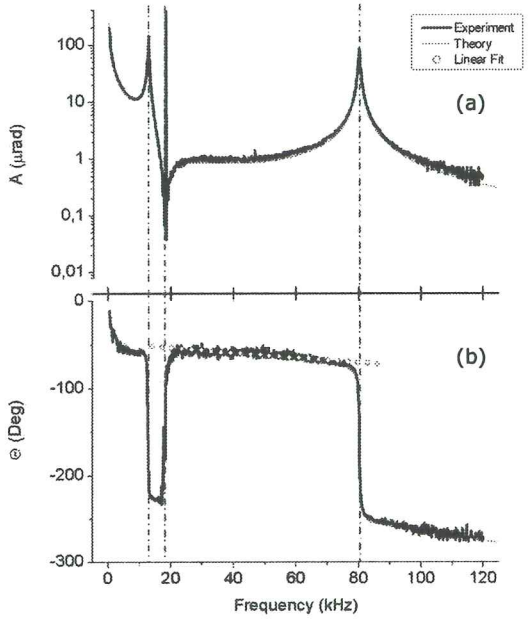

FIG. 4. (Color online) Experimental (thick line) and theoretical (thin line) graphs of the amplitude A [panel (a)] and phase Θ [panel b)], when the EX laser is focused in the middle of the cantilever; theoretical calculations are obtained for $L=350$ μm, $T=1.3$ μm, and $x_0=0.52L$. The slope amplitude of the linear fit (empty circles) accomplished on the experimental phase graph gives a temporal delay of $t_0=(0.78\pm0.03)$ μs.

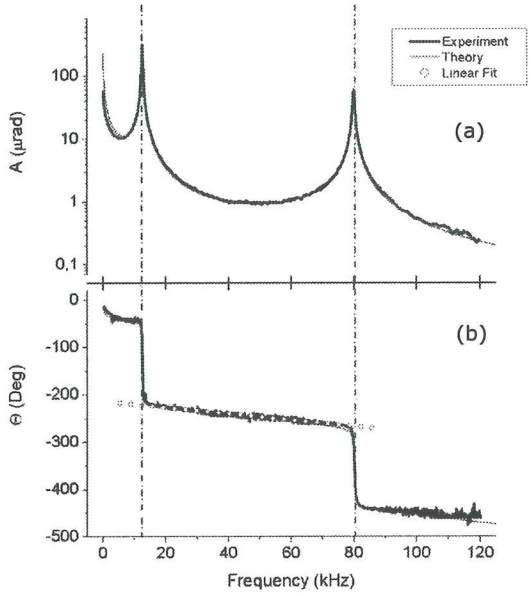

FIG. 5. (Color online) Experimental (thick line) and theoretical (thin line) frequency response of the amplitude A [panel (a)] and phase Θ [panel (b)] obtained considering the EX laser close the free end; theoretical calculations are obtained for $L=350$ μm, $T=1.3$ μm, and $x_0=0.76L$. The linear fit (empty circle) performed on the phase graph provides a temporal delay $t_0=(1.23\pm0.02)$ μs.

The amplitude of the first mode, $A_0(x_0)$, decreases monotonically with the distance whereas the second mode $A_1(x_0)$ is higher in the middle position.

This behavior can be interpreted taking into account that the photothermal effect is proportional to the second spatial derivative of the normal modes,[12] $d^2\phi_n(x)/dx^2$, that it is the observed trend for the first two modes as a function of the position.[15] Moreover, the amplitude graphs for the middle position [Fig. 4(a)] and near the tip [Fig. 5(a)] show, respectively, one and two antiresonance negative peaks just after the resonances. This behavior corresponds to a zero of the dynamical system under study, typical of multimodal systems, substantially due to the interfering coupling of several modes. Unlike the resonances that strictly depend on the geometrical and physical properties of the cantilever, the antiresonances also depend on the external forces.[20,21] This explains why changing the EX laser position (and therefore the external driving force) the antiresonances change their frequency or can even disappear: Fig. 3(a) does not show any antiresonance peak; in Fig. 4(a) there is one antiresonance occurring at $\approx$18 kHz; focusing the EX laser near the free end [Fig. 5(a)] two antiresonances are clearly visible for $\approx$13.6 kHz and $\approx$99.2 kHz.

The phase between the EX laser modulation and the deflection signal was also measured [see Figs. 3(b), 4(b), and 5(b)]. As expected, all the experimental phase graphs show a phase jump of 180° at the resonances and a variable phase shift at low frequencies depending on x_0. Particular attention has to be addressed to the antiresonance phase jumps because the fortuitous coupling of the modes near the zeros of the dynamics can lead to a second jump of 180° at the antiresonance peak, as in Fig. 5(b), but also to an inverse jump of −180° as in Fig. 4(b). Furthermore, the phase curve outside the jumps is not constant, but it shows a linear decay $\Theta=\Theta_0-2\pi t_0\nu$ indicating the presence of a constant delay t_0 between the EX laser modulation and the deflection detection [see Eq. (7)]. The value of t_0 was calculated for each position of the EX laser beam performing a fit to the linear regions.

The experimental results were compared with the solution of the cantilever dynamics obtained taking into account only the leading modes of the expansion in Eq. (3). In order to calculate the coefficients of Eq. (4), the only unknown parameter[22] was the optical absorbance, a multiplicative fac-

TABLE I. Amplitude and frequency of the cantilever resonances and antiresonances for three different EX laser positions; near the base ($x_0=0.1L$), in the middle ($x_0=0.52L$), and close to the tip ($x_0=0.76L$)

EX laser pos.	Base	Middle	Tip
1° *Res. Amp.* (μrad)	308.9	141.9	21.3
" Freq. (kHz)	12.65	12.55	12.65
1° *Antires.Amp.* (μrad)		0.115	0.281
" Freq. (kHz)		17.88	13.64
2° *Res.Amp.* (μrad)	59.2	82.0	24.8
" Freq. (kHz)	80.19	80.21	80.26
2° *Antires.Amp.* (μrad)			0.00784
" Freq. (kHz)			99.15

tor to the amplitude that stretches the vertical axis of the theoretical curve for A. This parameter was tuned in order to match the experimental curve.

Interestingly, to reproduce both amplitude and phase graphs, it was not sufficient to stop the expansion of Eq. (3) at the second mode (as expected taking into account that only two resonances are present in the amplitude graphs) but it was necessary to include five modes to accurately reproduce also the phase graphs.

V. CONCLUSIONS

In the present work, we experimentally studied the frequency dependence of the amplitude and phase of a vibrating cantilever excited by a modulated laser beam for three different positions of the EX laser. The system dynamics was theoretically modeled by means of an eigenmodes expansion[17,18] of the solution. The comparison between experimental and theoretical data show that photothermal excitation can be simply modeled starting from the heat diffusion equation and the resulting dynamics can be deeply described.

In addition, we observed that the accuracy of the proposed model is well verified around the resonance peaks by considering the first two spatial modes, but it is necessary to take into account up to five modes to achieve a good match at the anti-resonances for both amplitude and phase. This result becomes very crucial when dealing with the implementation of model-based control algorithms[23] because the stability of the system is connected to the confinement of the phase within a finite range.

*valerio.pini@imm.cnm.csic.es

[1] A. Alessandrini and P. Facci, Meas. Sci. Technol. **16**, R65 (2005).
[2] R. García and R. Pérez, Surf. Sci. Rep. **47**, 197 (2002).
[3] M. Allegrini, C. Ascoli, P. Baschieri, F. Dinelli, C. Frediani, A. Lio, and T. Mariani, Ultramicroscopy **42-44**, 371 (1992).
[4] N. Umeda, S. Ishizaki, and H. Uwai, J. Vac. Sci. Technol. B **9**, 1318 (1991).
[5] H. Yamashita, N. Kodera, A. Miyagi, T. Uchihashi, D. Yamamoto, and T. Ando, Rev. Sci. Instrum. **78**, 083702 (2007).
[6] T. Ando, T. Uchihashi, N. Kodera, D. Yamamoto, A. Miyagi, M. Taniguchi, and H. Yamashita, Eur. J. Physiol. **456**, 211 (2008).
[7] S. W. Stahl, E. M. Puchner, and H. Gaub, Rev. Sci. Instrum. **80**, 073702 (2009).
[8] D. Ramos, J. Mertens, M. Calleja, and J. Tamayo, Appl. Phys. Lett. **92**, 173108 (2008).
[9] T. E. Schäffer, J. P. Cleveland, F. Ohnesorge, D. A. Walters, and P. K. Hansma, J. Appl. Phys. **80**, 3622 (1996).
[10] M. Stark, R. Guckenberger, A. Stemmer, and R. W. Stark, J. Appl. Phys. **98**, 114904 (2005).
[11] M. P. Scherer, G. Frank, and A. W. Gummer, J. Appl. Phys. **88**, 2912 (2000).
[12] D. Ramos, J. Tamayo, J. Mertens, and M. Calleja, J. Appl. Phys. **99**, 124904 (2006).
[13] F. Quercioli, B. Tiribilli, C. Ascoli, P. Baschieri, and C. Frediani, Rev. Sci. Instrum. **70**, 3620 (1999).
[14] J. W. M. Chon, P. Mulvaney, and J. E. Sader, J. Appl. Phys. **87**, 3978 (2000).
[15] J. E. Sader, J. Appl. Phys. **84**, 64 (1998).
[16] D. Sarid, *Scanning Force Microscopy and Spectroscopy* (Oxford University Press, New York, 1994).
[17] M. V. Salapaka, H. S. Bergh, J. Lai, A. Majumdar, and E. McFarland, J. Appl. Phys. **81**, 2480 (1997).
[18] C. A. Van Eysden and J. E. Sader, J. Appl. Phys. **101**, 044908 (2007).
[19] R. R. Craig, *Structural Dynamics: An Introduction to Computer Methods* (Wiley, New York, 1981).
[20] F. J. Rubio-Sierra, R. Vázquez, and R. W. Stark, IEEE Trans. Nanotechnol. **5**, 692 (2006).
[21] R. Vázquez, F. J. Rubio-Sierra, and R. W. Stark, Nanotechnology **18**, 185504 (2007).
[22] The parameters used for the calculation were (subscripts 1 and 2 refer to gold and silicon, respectively): specific-heat capacity $c_{p_1}=130$ J/(Kg K), $c_{p_2}=700$ J/(Kg K); mass density $\rho_1=19\,300$ Kg/m^3, $\rho_2=2329$ Kg/m^3; thermal conductivity $\kappa_1=310$ W/(mK), $\kappa_2=163$ W/(mK); Young's modulus $E_1=80\times10^9$ Pa, $E_2=170\times10^9$ Pa; thermal expansion coefficient $\alpha_1=14.2\times10^{-6}$ m/K, $\alpha_2=3.2\times10^{-6}$ m/K; thickness $t_1=70\times10^{-9}$ m, $t_2=1.3\times10^{-6}$ m; heat-transfer coefficient $h_1=h_2=10$ W/(m^2 K).
[23] V. A. Spector and H. Flashner, J. Dyn. Sys. Meas., Control **112**, 186 (1990).